Plant Elongator regulates auxin-related genes during RNA polymerase II transcription elongation

Hilde Nelissen[a,1], Steven De Groeve[a,1], Delphine Fleury[a,b], Pia Neyt[a], Leonardo Bruno[c], Maria Beatrice Bitonti[c], Filip Vandenbussche[d], Dominique Van Der Straeten[d], Takahiro Yamaguchi[e,f], Hirokazu Tsukaya[e,f], Erwin Witters[g], Geert De Jaeger[a], Andreas Houben[h], and Mieke Van Lijsebettens[a,2]

[a]Department of Plant Systems Biology, Flanders Institute for Biotechnology, and Department of Plant Biotechnology and Genetics, Ghent University, 9052 Ghent, Belgium; [b]Australian Centre for Plant Functional Genomics, University of Adelaide, Glen Osmond, SA 5064, Australia; [c]Laboratory of Botany, Department of Ecology, Università della Calabria, 87030 Arcavacata di Rende, Italy; [d]Unit Plant Hormone Signaling and Bio-imaging, Department of Physiology, Ghent University, 9000 Ghent, Belgium; [e]National Institute for Basic Biology, Okazaki, Aichi 444-8585, Japan; [f]Graduate School of Science, University of Tokyo, Tokyo 113-0033, Japan; [g]Department of Biology, University of Antwerp, 2020 Antwerp, and Flemish Institute for Technological Research, 2400 Mol, Belgium; and [h]Leibniz Institute of Plant Genetics and Crop Plant Research, 06466 Gatersleben, Germany

Communicated by Marc C. E. Van Montagu, Ghent University, Ghent, Belgium, December 1, 2009 (received for review July 6, 2009)

In eukaryotes, transcription of protein-encoding genes is strongly regulated by posttranslational modifications of histones that affect the accessibility of the DNA by RNA polymerase II (RNAPII). The Elongator complex was originally identified in yeast as a histone acetyltransferase (HAT) complex that activates RNAPII-mediated transcription. In *Arabidopsis thaliana*, the Elongator mutants *elo1*, *elo2*, and *elo3* with decreased leaf and primary root growth due to reduced cell proliferation identified homologs of components of the yeast Elongator complex, Elp4, Elp1, and Elp3, respectively. Here we show that the Elongator complex was purified from plant cell cultures as a six-component complex. The role of plant Elongator in transcription elongation was supported by colocalization of the HAT enzyme, ELO3, with euchromatin and the phosphorylated form of RNAPII, and reduced histone H3 lysine 14 acetylation at the coding region of the *SHORT HYPOCOTYL 2* auxin repressor and the *LAX2* auxin influx carrier gene with reduced expression levels in the *elo3* mutant. Additional auxin-related genes were down-regulated in the transcriptome of *elo* mutants but not targeted by the Elongator HAT activity showing specificity in target gene selection. Biological relevance was apparent by auxin-related phenotypes and marker gene analysis. Ethylene and jasmonic acid signaling and abiotic stress responses were up-regulated in the *elo* transcriptome and might contribute to the pleiotropic *elo* phenotype. Thus, although the structure of Elongator and its substrate are conserved, target gene selection has diverged, showing that auxin signaling and influx are under chromatin control.

Arabidopsis | chromatin | histone acetyltranferase complex | SHY2

In plants, growth and form are determined by the spatial and temporal regulation of cell division and cell expansion in which plant hormones play a crucial role. The plant hormone auxin is a major integrator of stimuli to steer cell expansion and, hence, growth. In addition, its polar distribution results in concentration gradients and maxima that are interpreted by specific cells through a nuclear signaling pathway, leading to transcriptional changes and the onset of specific developmental programs, such as primary root apical meristem maintenance and daughter cell specification, lateral root initiation and gravitropism, leaf vascular patterning, and leaf and flower initiation and positioning (1). Auxin enhances the affinity of TIR1 for AUX/IAAs (2, 3), which leads to their ubiquitination by the SCF^{TIR1} E3 ligase (4), their subsequent degradation by the proteasome, and complex transcriptional reprogramming through the AUXIN RESPONSE FACTOR (ARF) transcription factors. Mutants in signaling components, such as *bodenlos* (*bdl*, BDL/IAA12) and *short hypocotyl 2* (*shy2*, SHY2/IAA3), are defective in proximo-distal axis formation as visualized by a short primary root and reduced shoot apical dominance (5, 6). Components of the cellular auxin transport machinery are transmembrane influx (AUX1/LAX1) and efflux (PIN1–PIN8) carriers in addition to P-glycoproteins (PGPs) of the ABCB transporter family (1). Crosstalk of auxin signaling with other hormone signaling pathways, such as ethylene, provides other levels of complexity to the plant for developmental programming upon environmental and endogenous stimuli. The integration of such developmental programs together with metabolic and physiological pathways contributes to the complex trait of growth in plants. Their transcriptional or translational control mechanisms are well studied, but much less is known about their epigenetic regulation; i.e., the histone code and the genomic DNA methylation state also regulate gene expression and change in response to developmental and environmental cues (7).

We studied the genetic and epigenetic regulation of growth in the model plant *Arabidopsis thaliana* by using the leaf as an experimental system. Leaf mutants with narrow and elongated lamina shape allowed the identification of the plant homologs of the yeast Elongator complex components (8). In yeast and humans, Elongator consists of the core subcomplex composed of ELP1, ELP2, and ELP3 and the accessory subcomplex containing ELP4, ELP5, and ELP6 (9, 10). The copurification of the Elongator complex with the phosphorylated RNA polymerase II (RNAPII) (11) and the in vivo histone acetyl transferase (HAT) activity (12) suggested a role for the complex in RNAPII transcription elongation in yeast (11, 12). The yeast Elongator complex was also reported to have a function in exocytosis, tubulin acetylation, and tRNA modification. In yeast, the Elongator mutants slowly adapt to changes in growth conditions, whereas in humans, they cause a neuronal disease, called familial dysautonomia (13). In mammals, genes involved in cell motility and fibroblast and embryogenic development were found to be direct targets for acetylation by the Elongator complex during transcription elongation (14, 15), whereas in yeast no direct transcriptional targets of the complex were identified thus far.

Here we show that the structure of the Elongator complex as well as its function in RNAPII transcription elongation is conserved in plants. Auxin-related phenotypes in the *elo* mutants correlated with reduced acetylation of H3K14 in auxin biology-related genes, revealing a plant-specific target process and genes for Elongator.

Author contributions: H.N., S.D.G., L.B., and M.V.L. designed research; H.N., S.D.G., D.F., P.N., L.B., F.V., T.Y., and E.W. performed research; H.N., S.D.G., D.F., L.B., M.B.B., D.V.D.S., H.T., E.W., G.D.J., A.H., and M.V.L. analyzed data; and H.N., S.D.G., and M.V.L. wrote the paper.

The authors declare no conflict of interest.

[1]H.N. and S.D.G. contributed equally to this work.

[2]To whom correspondence should be addressed at: Department of Plant Systems Biology, VIB, Ghent University, Technologiepark 927, 9052 Ghent, Belgium. E-mail: mieke.vanlijsebettens@psb.vib-ugent.be.

This article contains supporting information online at www.pnas.org/cgi/content/full/0913559107/DCSupplemental.

Results and Discussion

Elongator Complex Purification in Plant Cell Cultures. In *Arabidopsis*, the phenotypic resemblance of the different knockdown *elongator* (*elo*) mutants, the clustering of their transcriptome, and their epistatic interactions (8) suggested that the ELO proteins function in a complex. To verify the existence and composition of an Elongator complex in plants, a tandem affinity purification (TAP) was done on extracts of *Arabidopsis* cell suspension cultures, transformed with overexpression constructs for *ELO3* fused to IgG domains and the streptavidin-binding peptide (GS-TAP) of protein G. The wild-type phenotype was restored after transformation of the *elo3-1* mutant with the tagged *ELO3* construct, showing its functionality. Two purifications with p35S-GStag-ELO3 were separated on polyacrylamide gels and stained with Coomassie Brilliant Blue (Fig. S1*A*). Subsequently, the entire gel lanes were sliced in fragments and sequenced by mass spectrometry that revealed the presence of ELO2, AtELP2, ELO3, ELO1, AtELP5, and AtELP6 (Tables S1 and S2), corresponding to the homologs of the six Elongator components in yeast. All six components were purified in other TAPs with ELO1, ELO3, and AtELP5 as bait (Tables S1 and S2). The plant homologs of the yeast Elongator as identified through mutational analysis and BLAST search interacted in vivo and that besides the previously described ELO proteins (8), the three components encoded by At1g49540, At2g18410 and At4g10090 (16) could now be annotated as the Elongator components, *AtELP2*, *AtELP5*, and *AtELP6*, respectively. Stoichiometric concentrations of ELO1, AtELP5, and AtELP6 were found on gels with the tagged ELO1 or AtELP5 as bait when compared to the lower concentrations of ELO2, AtELP2, and ELO3; in contrast, with ELO2 as bait, only stoichiometric concentrations of AtELP2 and ELO3 could be detected. These data suggest that the plant Elongator complex also consists of two discrete subcomplexes as was put forward for yeast (9). Pairwise yeast two-hybrid analysis revealed that ELO1 interacted with AtELP6, but not with AtELP5, whereas AtELP5 interacted with AtELP6, but not with ELO1 (Fig. S1 *B–E*). In summary, an Elongator complex is formed in plants with a structure similar to that in yeast and humans.

GFP-ELO3 Protein Localization in Euchromatic Regions in Interphase Nuclei. As all Elongator components copurify with ELO3, it was used to investigate the subcellular localization of the complex in plants. ELO3 contained a GCN5-related *N*-acetyltransferase family domain with a very high homology (67% identity and 80% similarity) with its yeast counterpart, hinting at functional conservation. Linking of the green fluorescent protein (GFP) to the N terminus of ELO3 did not abolish its function, because the mutant phenotype in *elo3-1* and *elo3-6* was restored to the wild type upon transformation. Several independent T2 transgenic plants overexpressing the *GFP-ELO3* fusion gene were analyzed. The GFP-ELO3 fusion protein was localized predominantly in the nucleus and, to a lesser extent, in the cytoplasm (Fig. 1*A*). The red fluorescent dye *N*-(3-triethylammoniumpropyl)-4-(p-diethylaminophenylhexatrienyl)-pyridinium 2Br (FM4-64) facilitated the visualization of the tissue context and did not overlap with GFP fluorescence, indicating that ELO3 was not located in the plasma membrane. Deconvolution microscopy for superior optical resolution of globular structures was applied to nuclei in root tissues and revealed the nonhomogenous nucleus-localized GFP-ELO3 fluorescence. Big and small "signal holes" that putatively represented the nucleolus and heterochromatic chromocenters, respectively (Fig. 1*B*), were analyzed by colocalization studies of GFP-ELO3 with immunodetection of dimethylated histone H3 labeling at lysine 4 (H3K4me2) (Fig. 1*C*), an atypical histone mark associated with euchromatin in *Arabidopsis* (17), of dimethylated histone H3 at lysine 9 (H3K9me2) antibody (Fig. 1*D*), a histone mark diagnostic for heterochromatin (18),

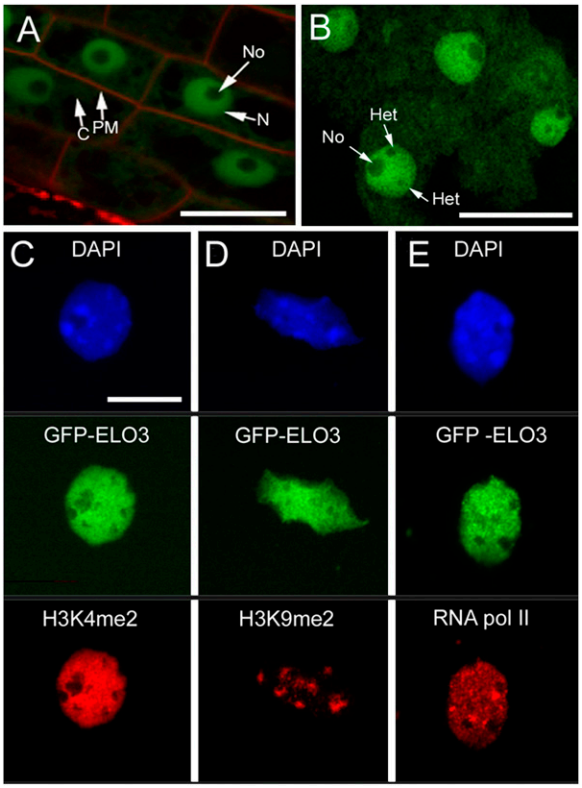

Fig. 1. Localization of the GFP-ELO3 fusion protein and euchromatin colocalization in 4C interphase nuclei of *Arabidopsis*. (*A* and *B*) Transgenic primary root tissue of 4-day-old seedlings, visualized with confocal microscopy (*A*) and deconvolution microscopy (*B*). C, cytoplasm; Het, heterochromatin; N, nucleus; No, nucleolus; PM, plasma membrane. (Scale bars: 20 μm in *A* and *B*.) (*C*) Anti-GFP and anti-histone H3K4me2 sera examination of the presence of ELO3 and transcriptionally potent chromatin on interphase nuclei by indirect immunofluorescence. (*D*) Heterochromatic regions detected with anti-histone H3K9me2, not overlapping with the localization of GFP-ELO3. (*E*) Double immunolabeling with anti-RNAPII and anti-GFP to reveal a potential link between gene transcription and localization of GFP-ELO3. Most of the brightly DAPI-stained heterochromatic regions revealed a reduced labeling of GFP-ELO3, anti-histone H3K4me2, and RNAPII. In all combinations, the genomic DNA was visualized by DAPI staining. DAPI fluorescence is blue, GFP antibody signal is green, and the other antibody signals are red. (Scale bar: 5 μm in *C–E*.)

and of the labeled phosphorylated large subunit of eukaryotic RNAPII, which catalyzes transcription elongation of most eukaryotic genes into mRNA. The immunofluorescence pattern of GFP-ELO3 overlapped with that of H3K4me2 and the phosphorylated large subunit of eukaryotic RNAPII, whereas the brightly 4′,6-diamidino-2-phenylindole (DAPI)-stained heterochromatic chromocenters remained unlabeled. In contrast, the GFP-ELO3 and H3K9me2 signals were almost mutually excluded. The signal pairs GFP-ELO3/H3K4me2 and GFP-ELO3/RNAPII overlapped and had a similar profile in contrast to the GFP-ELO3/H3K9me2 signals that did not match well (Fig. S2). The data indicate that the Elongator complex is involved in the process of RNAPII transcription elongation in plants and that its nuclear function in transcription is conserved between yeast (11), humans (12), and plants.

***ELO* Genes Are Expressed in Meristems.** The spatial and temporal expression patterns of the *ELO1*, *ELO2*, and *ELO3* genes were identical and shown only for *ELO3* (Fig. 2). High transcript accumulation was observed in the shoot apical meristem, the emerging leaf primordia, and provascular strands of young seed-

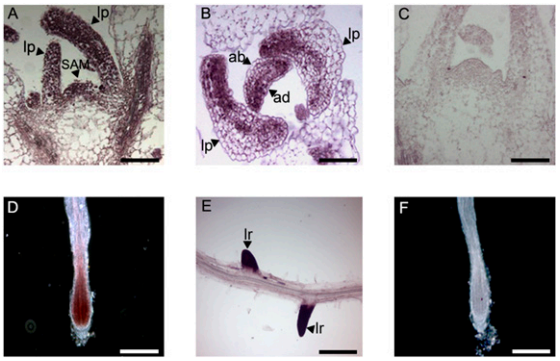

Fig. 2. In situ hybridization pattern of *ELO3* antisense probe. (*A*) Longitudinal section of 14-day-old shoot apical meristem and early leaf primordia. (*B*) Cross section of 14-day-old leaf primordia. (*C*) Longitudinal section of 14-day-old shoot apical meristem and early leaf primordia hybridized with *ELO3* sense probe. (*D*) Whole-mount hybridization of 14-day-old primary root. (*E*) Whole-mount hybridization of 14-day-old lateral roots. (*F*) Whole-mount hybridization of 14-day-old primary root with *ELO3* sense probe. ab, abaxial surface; ad, adaxial surface; lp, leaf primordium; lr, lateral root; SAM, shoot apical meristem. (Scale bars: *A–C*, 70 μm; *D–F*, 100 μm.)

lings (Fig. 2 *A* and *B*), at the adaxial side of leaf primordia (Fig. 2*B*), in primary and lateral root meristems (Fig. 2 *D* and *E*), and throughout the young, developing floral bud, especially in the reproductive and vascular tissues. No transcripts were detected in the differentiated zones of primary and lateral roots (Fig. 2 *D* and *E*). In conclusion, *ELO* genes were expressed in meristematic tissues, such as shoot apices, root tips, and adaxial sides of leaf primordia that determine cell proliferation and growth. Hence, the reduced cell proliferation in *elo* mutants (8) can be explained by a depletion of the Elongator complex, specifically in meristematic and dividing tissues. On the basis of the conservation of the *ELO3* HAT and its colocalization with euchromatin and phosphorylated RNAPII (Fig. 1), we conclude that Elongator is a putatively positive regulator of mRNA transcription in dividing tissues.

Modulation of Auxin-Related Gene Expression in *elo* Mutants. As histone acetylation positively affects the RNAPII transcription efficiency (7), we analyzed the gene classes down-regulated in the *elo* mutants to identify plant-specific pathways targeted by Elongator that might explain the phenotypes of the *elo* mutants. Microarray analyses on shoot apices of *elo* and Landsberg *erecta* (L*er*) seedlings previously indicated that the *elo* mutants clustered together in one group of differentially expressed genes (8). In the same data set, the overrepresented Gene Ontology (GO) categories of the genes specifically down-regulated in the *elo* mutants were analyzed with BiNGO (19). A restricted number of significant classes ($P < 0.001$) was obtained: chromatin assembly, pattern specification, vascular tissue development, and response to auxin stimulus. Most strikingly, a large number of primary and secondary auxin response genes were present, i.e., two *SAUR*, *IAA14/SLR*, *IAA13*, *IAA11*, *ATHB8*, *IAA3/SHY2*, *IAA12/BDL*, *ARF10*, *ARF11*, *ARF18*, *ACL5*, in addition to auxin biosynthesis (*TAR2*), and auxin transport (*LAX2* and *PIN4*). The aldehyde oxidase 1, involved in auxin biosynthesis, auxin transporters (*PGP1* and *PGP4*), and auxin-responsive genes were up-regulated (Table S3). The auxin metabolism, transport, perception, and signaling were severely affected in the *elo* mutants and could be responsible for the leaf and root growth phenotypes observed in the *elo* mutants (8).

Auxin Biology-Related Phenotypes in *elo* Mutants. Previously, the *elo* mutants were described with narrow leaves and a short primary root (8). To verify whether the reduced expression of auxin biology-related genes in the *elo* mutants is biologically relevant, apical dominance, inflorescence phyllotaxis, leaf venation patterning, and lateral root density were studied in the strong *elo1-1*, *elo2-1*, and *elo3-1* and the weak *elo1-10* and *elo3-10* alleles of L*er* and Columbia-0 (Col-0), respectively.

In wild-type *Arabidopsis*, the modulation of auxin transport capacity in the main stem has been proposed to regulate bud outgrowth (20). In the *elo* mutants, apical dominance was clearly reduced, resulting in a precocious growth stop of the primary inflorescence and an overgrowth of the secondary branches, relative to the primary inflorescence (Fig. 3 *A–C*, Fig. S3*A*). This reduced apical dominance in the *elo* mutants supports a defective auxin biology. The position of lateral organs, the phyllotaxis, is determined by auxin maxima at the shoot or inflorescence meristems and results in a spiral in *Arabidopsis* (21). In the *elo* mutants, the phyllotaxis is defective with secondary inflorescences originating at the same node or ectopically causing irregular internode length (Fig. 3 *A* and *B*), indicating that the auxin maxima were not properly established in the *elo* mutants and suggesting a role for Elongator in auxin distribution or signaling. Such defects also occurred in the *shy2-2* mutants (Fig. S3*B*). Secondary branches that are subtended by cauline leaves in wild-type *Arabidopsis* were

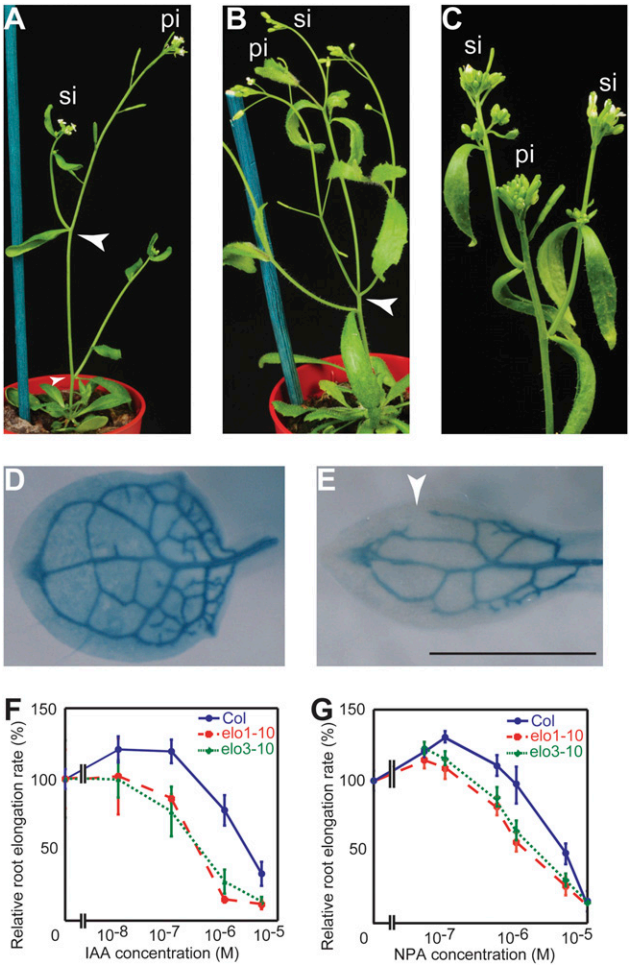

Fig. 3. Auxin-related phenotypes in *elo* alleles. (*A*) Wild-type inflorescence. (*B*) *elo3-6* showing altered phyllotaxis of the secondary inflorescence branches (arrowheads). (*C*) *elo1-1* showing reduced apical dominance. (*D*) Venation pattern visualized by X-Gluc histochemical assay of wild type. (*E*) *elo3-1* mutant transformed with p*ATHB8-GUS* showing open venation (arrowhead). (*F* and *G*) Primary root length on increasing levels of exogenously applied IAA (*F*) and NPA (*G*). Pi, primary inflorescence; si, secondary inflorescence. (Scale bar: 1 mm.)

often absent in the *elo* mutants (Fig. 3*B*). The putative ectopic auxin accumulation could be the consequence of a defect in the auxin transport and relate to the differentially expressed auxin-related genes in *elo* mutants (Table S3). The p*ATHB8-GUS* marker for the provascular cell state revealed a defective venation patterning in the *elo* mutants, with disconnected primary loops and reduced secondary and tertiary veins, which is typical for an altered auxin distribution (Fig. 3 *D* and *E*) (22).

Auxin signaling affects primary and lateral root growth; mutants of the *AUX/IAA* auxin response-related genes have a very short primary root (5, 6). Similarly, in the *elo* mutants, primary roots were severely reduced (8) and often grew agravitropically, with a significantly reduced lateral root density (number of lateral roots/cm): 1.7 ± 0.9 in *elo1-1* and 1.4 ± 1.1 in *elo3-1* mutants versus 2.5 ± 0.6 in the L*er* control. In addition, ectopic lateral roots were observed in *elo2-1* (Fig. S3 *D* and *E*). Thus, the short primary root, the low lateral root density, and the ectopic lateral roots observed in the *elo* mutants argue also for a defect in auxin signaling or distribution.

The weak *elo1-10* and *elo3-10* alleles in which the primary root growth was not severely compromised were used to investigate the effect of increasing levels of exogenously applied IAA and the auxin transport inhibitor *N*-1-naphthylphthalamic acid (NPA). Low concentrations of both supplied chemicals reduced growth in the *elo* mutants, suggesting that the endogenous level of auxin was higher in the *elo* mutants and that the auxin transport was compromised in the mutants (Fig. 3 *F* and *G*). Levels of free IAA were determined in shoot apices of 14-day-old seedlings that coincide with sites of auxin biosynthesis. The free IAA concentration was threefold higher in *elo2-1* than in L*er* (Fig. S4*A*), possibly interfering with the autoregulation of the shoot apical meristem and the reason for the, sometimes, extremely fasciated inflorescence stems in the *elo* mutants (Fig. S3*C*).

Hormonal Misregulation Might Contribute to the Pleiotropic Phenotype of the *elo* Mutants. In each of the *elo* mutants, the ethylene emanation increased significantly (Fig. S4*B*) and the jasmonic acid (JA) content in the *elo2-1* mutant increased as well (Fig. S4*C*), which correlated with the transcriptional up-regulation of ethylene-responsive genes (*AP2/ERF*), JA biosynthesis genes (*ACX1*, *AOS*, *LOX1*, and *LOX2*), and two major JA response genes (*VSP1* and *COR1*) (Table S3). It is not clear whether the increased biosynthesis of ethylene and JA is the consequence of elevated auxin levels. However, increased JA might contribute to the short root phenotype of the *elo* mutants and the down-regulation of histone genes in the GO category chromatin assembly of their transcriptome because exogenous addition of JA reduces replication, root growth, and histone gene expression (23, 24). The GO categories abiotic stress, defense to pathogen, and anthocyanin biosynthesis were significantly up-regulated in the microarray data set, which might be the consequence of JA or ethylene overproduction in the *elo* mutants. This observation correlates with the previously identified *abo1/elo2* allele as abscisic acid (ABA) hypersensitive drought-resistant phenotype (25) and with resistance of *elo* mutants to oxidative stress produced by methyl viologen and increased anthocyanin biosynthesis (26).

Elongator Targets Specific Genes Related to Auxin Biology. On the basis of the *elo* phenotypes and the transcriptome, we identified a number of genes with reduced expression levels (Table S3) as putative targets of Elongator, i.e., the *SHY2/IAA3* and *BDL/IAA12* repressors, the *ATHB8* auxin response gene (22), the *LAX2* influx carrier, the *PIN4* efflux carrier, and the *AP2/ERF* ethylene response gene. The down-regulation of these genes in the *elo* mutants was verified with quantitative (q)PCR (Fig. 4*D* and Fig. S5*E*). We investigated whether the reduced expression of the selected genes was related to reduced acetylation levels of histone H3 lysine-14 in their promoter and/or coding regions

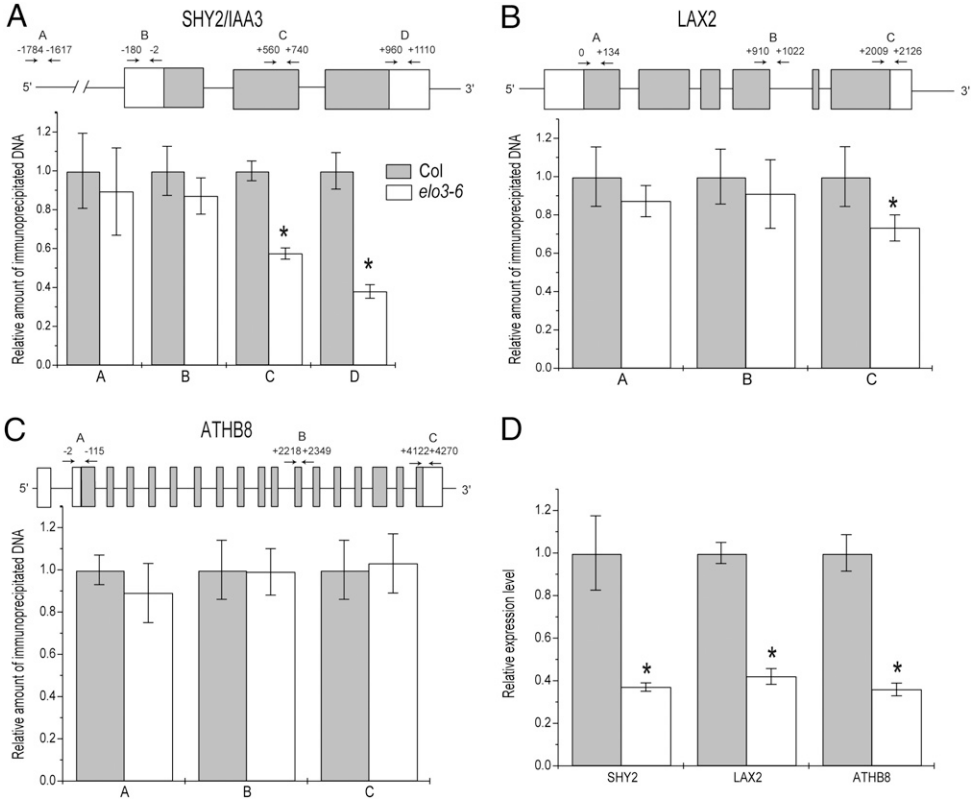

Fig. 4. ChIP analysis of H3K14 acetylation at *SHY2/IAA3* (*A*), *LAX2* (*B*), and *ATHB8* (*C*) genes and relative expression level in *elo3-6* (*D*). Gene structure and position of primers relative to the initiation ATG codon are indicated. Open and shaded boxes are untranslated sequences and exons, respectively. The relative amount of immunoprecipitated chromatin fragments as determined by real-time PCR was compared to the wild type (arbitrarily given as 1). Error bars represent SD values of at least three repetitions. *, significant differences between wild type and mutant according to a *t* test ($P < 0.05$).

because H3K14 is the predominant substrate of the ELP3 HAT in yeast (12). DNA of the *elo3-6* mutant and Col-0 wild type, immunoprecipitated with an antibody against acetylated H3K14 or histone H3, was normalized by using a primer pair specific for the 5′ end of *ACTIN2/7*, a constitutively expressed gene. qPCR after chromatin immunoprecipitation (ChIP) with antibodies against H3K14Ac was used as a measure for the amount of acetylated H3K14, but remained unchanged at the promoter and coding sequence of the *ACTIN2/7* gene between the *elo3-6* mutant and the wild type (Fig. S5*A*). qPCR after ChIP showed significantly reduced levels with primers corresponding to the coding and 3′-untranslated regions of the *SHY2/IAA3* gene in the *elo3-6* mutant and normal levels with primers against the upstream and core promoter regions (Fig. 4*A*). Similarly, qPCR levels with primers in the 3′-untranslated region of the *LAX2* gene were significantly lower in the *elo3-6* mutant (Fig. 4*B*), but did not differ with primer pairs for *ATHB8* (Fig. 4*C*), *PIN4*, *BDL/IAA12*, and *AP2/ERF* (Fig. S5*B–D*), indicating that the decreased expression level was an indirect effect of the *elo* mutation. In summary, the reduced H3K14 acetylation levels at the coding and 3′-untranslated regions of the *SHY2/IAA3* and *LAX2* genes in the *elo* mutants explained the lowered expression levels and identified these genes as direct targets for Elongator HAT activity during RNAPII transcription elongation. Indeed, our analysis shows that the Elongator complex targets specific genes for acetylation and transcriptional regulation rather than affecting transcription generally, which adds important mechanistic information on the Elongator function in transcription.

Conclusion

We demonstrated that the protein structure of the Elongator complex is conserved from yeast and mammals to plants. Our data suggest a role of Elongator in RNAPII transcription elongation in plants through ELO3 (GCN5 HAT family) acetylation of H3K14 in coding and 3′-untranslated regions of specific genes, such as *SHY2/IAA3* and *LAX2*. These genes are part of auxin-related processes that are plant specific. Hence, the function of Elongator, although conserved in substrate selection, evolved in plants with respect to target preference. Besides the target of the ELO3 HAT, the *SHY2/IAA3* gene is also the target of the GCN5 HAT that acetylates specifically its promoter (27), suggesting a complex chromatin-related control for this gene.

Several genes, which are induced by external stimuli that provoke cellular responses, are regulated at the level of transcription elongation (28). For these genes, the RNAPII initiation complex is stalled or paused in the proximity of the promoters in the absence of the appropriate stimulus. Upon stimulation, the C-terminal domain of the RNAPII gets phosphorylated and transcription elongation is resumed, allowing a fast response. In this manner, transcription elongation factors are thought to control the transcription rates of early response genes in a stimulus- and gene-specific way (29). Also in *Arabidopsis*, GCN5 acetylates gene subsets in a stimulus-dependent manner, although the exact mechanism of gene specificity remains to be established (30). Our working hypothesis puts the Elongator complex forward as a factor that steers the transcription elongation of a subset of early response genes, regulated by signals from the environment. Auxin-induced expression of *SHY2/IAA3* was not affected in the *elo* mutants (Fig. S6), indicating that ARF-mediated gene activation of *SHY2/IAA3* acts independently of the Elongator pathway. The Elongator complex might not react to the auxin stimulus, might be dose dependent, or might be responsible only for basal transcription of this gene.

The Elongator-dependent chromatin-mediated regulation of the auxin signaling gene *SHY2/IAA3* and the auxin influx carrier *LAX2* might, in part, explain the auxin-related phenotypes observed in the *elo* mutants: Both gain-of-function and loss-of-function alleles of *shy2* display short primary roots, whereas only the gain-of-function mutation reduces lateral root formation (5). Thus, the decreased lateral root formation in the *elo* mutants cannot simply be explained by a down-regulation of *SHY2/IAA3*. It was hypothesized that *shy2* mutations might alter the auxin transport (5); therefore, the combinatorial down-regulation of both *SHY2/IAA3* and *LAX2* in the *elo* mutants might result in a severely aberrant auxin distribution. In the triple *lax* mutant, the auxin distribution is disturbed, with decreased angles of phyllotaxis and narrow leaf shapes (31), which are also typical phenotypes of the *elo* mutants. In addition, up-regulation of JA, ethylene, and abiotic stress-related genes might contribute to other aspects of the *elo* phenotype, such as reduced DNA replication and, hence, lessened cell proliferation (8) and resistance to abiotic stress (26). In analogy with the high number of target genes of the GCN5 HAT (30), it is expected that the majority of the direct targets of the Elongator complex still has to be identified, which will allow us to get the complete picture of the molecular mechanisms underlying the *elo* phenotypes.

Materials and Methods

Plant Material and Growth Conditions. The mutants *elo1-1*, *elo2-1*, and *elo3-1* (8) were in L*er*, the *elo3-6* mutant in Col-0 (GABI-KAT collection code GABI555_H06), and the *elo1-10* and *elo3-10* in Col-0 were isolated from an x-ray-irradiated M2 population (line 111) and a T-DNA-mutagenized T2 population (line 2018), respectively. In *elo1-10*, the genomic region was deleted, including the fifth exon to the 3′ end of the *ELO1* gene and, in *elo3-10*, a single-base deletion occurred at 2452A of the *ELO3* gene, resulting in a frameshift and a premature stop codon with 28 amino acid residues. The p*ATHB8-GUS* line (N296) was obtained from the Nottingham Arabidopsis Seed Stock Centre. The growth chamber conditions were 16 h/8 h (day/night) with white light (neon tubes, cool white), 100 $\mu mol \cdot m^{-2} \cdot s^{-1}$ light intensity, and 20°C.

In Situ Hybridization. Short and specific (GSTs) fragments of *ELO1* (At3g11220), *ELO2* (At5g13680), and *ELO3* (At5g50320) genes were cloned in the pGEM-T-Easy vector (Promega). Digoxigenin (DIG)-labeled RNA sense and antisense probes were synthesized by T7 and SP6 polymerase-driven in vitro transcription, respectively (DIG-RNA labeling kit protocol; Roche Diagnostics).

Root tips, shoot apices and leaves, and floral buds were excised from 7-, 12-, and 20-day-old L*er* seedlings, respectively, fixed, dehydrated, embedded in paraffin, cut into 8-μm sections, and hybridized (55°C) to a DIG-labeled antisense RNA probe as described (32). Transcript accumulation was visualized as a violet-brown staining.

Microarray Analysis. Shoot apices consisting of the shoot apical meristem and first and second leaf primordia at the petioleless stage of seedlings between 11 and 18 days after germination in vitro were harvested. RNA was extracted with the TriZOL method (Invitrogen). ATH1 Affymetrix chips were used for hybridization (8) and the data are available on ArrayExpress (E-MEXP-300). The molecular processes affected specifically in the *elo* mutants were obtained by subtracting the differentially expressed transcripts also present in the *drl1-2* and *hub1-1* (8, 33) mutants, two narrow-leaf mutants in which transcriptomics were analyzed simultaneously.

Tandem Affinity Purifications. The TAP tag was fused C-terminally (ELO1 and AtELP5) or N-terminally (AtELP2 and ELO3) to the various cDNA clones expressed from the 35S promoter and transformed in wild-type *Arabidopsis* cell suspension cultures (PSB-D). The TAP was carried out as described (34, 35) with minor modifications: 300 mM NaCl in the extraction buffer and two subsequent centrifugation steps at 47,807 × *g* after extraction (omitting the ultracentrifugation step). Total protein extract (200 mg) was loaded on the IgG column. Eluted proteins were separated on 4–12% NuPAGE gels; the entire gel lanes were cut into fragments and analyzed by Maldi-TOF-TOF-MS. To increase the stringency of the data set, contaminating proteins due to experimental background were systematically subtracted from the copurified protein lists. Proteins with a probability-based identity of at least 95% and present in at least two independent TAP experiments were retained as interactors. Therefore, no other proteins represented by additional bands on the gel could be assigned as Elongator components or interactors.

Localization of GFP-ELO3 in Plant Cells. Plants were grown vertically in vitro for 4 days and primary roots analyzed with a confocal microscope 100M with the software package LSM 510 version 3.2 (Zeiss). GFP fluorescence was imaged at 488 nm excitation. Emission fluorescence was captured in the frame-scanning mode, alternating GFP fluorescence via a 500- to 550-nm bandpass emission

filter. The FM4-64 dye (5 μg/mL) that intercalates into the plasma membrane was imaged at 511 nm excitation to visualize the tissue context.

Deconvolution microscopy was used for superior optical resolution of globular structures. Each photograph was collected as a sequential image along the *z* axis with ≈11 slices per specimen. All images were collected in gray scale and pseudocolored with Adobe Photoshop. Projections (maximum intensity) were done with the program AnalySIS (Soft Imaging System).

Analysis of the Nuclear Proteins by Indirect Immunofluorescence. Replicated (4C) nuclei of young *Arabidopsis ELO3-GFP* leaf tissue were immunostained and analyzed as described previously (18). The following primary antibodies were used: rabbit anti-RNA polymerase II CTD phospho Ser5 (Active Motif; diluted 1:100), mouse monoclonal anti-GFP (Roche; diluted 1:100), rabbit anti-histone H3K4me2 (Upstate Biotechnology; diluted 1:300), and rabbit anti-histone H3K9me2 (Upstate Biotechnology; diluted 1:300).

ChIP. ChIP was done as described previously with minor modifications (36). Seeds of Col-0 and the *elo3-6* mutant were sown on Murashige and Skoog medium and grown in vitro under short-day conditions. Seedlings were harvested after 3 weeks, fixed in 1% formaldehyde for 10 min in a vacuum, and neutralized by 0.125 M glycine for 5 min. Samples were ground in liquid nitrogen and nuclei were isolated and lysed in the presence of protease inhibitors. The isolated chromatin was sonicated five times for 30 s in a Branson sonifier water bath. The antibodies for immunoprecipitation were purchased from Upstate Biotechnology: anti-histone H3K14Ac (07-353) and anti-histone H3 (05-499). Immunoprecipitated DNA was purified with the Roche PCR Purification Kit, dissolved in 50 μL supplemented with RNase A, and analyzed by real-time PCR (Bio-Rad iCycler) with primers in the promoter and coding regions of the tested genes (*SI Text*; Fig. 4 and Fig. S5).

ACKNOWLEDGMENTS. We thank J. Fuchs for flow-sorting of nuclei and K. Kumke for technical assistance; G. Persiau, E. Van De Slijke, and D. Eeckhout for help with TAP and MS; E. Prinsen for IAA and JA measurements; and M. De Cock for help in preparing the manuscript. This work was supported by the European Research Training Network (contract no. HPRN-CT-2002-00267), the Institute for the Promotion of Innovation through Science and Technology in Flanders ("Generisch Basisonderzoek aan de Universiteiten," grant 20193). H.N. and S.D.G. are indebted to the Institute for the Promotion of Innovation through Science and Technology in Flanders for a postdoctoral and a predoctoral fellowship, respectively. F.V. is a postdoctoral fellow of the Research Foundation-Flanders.

1. Vanneste S, Friml J (2009) Auxin: A trigger for change in plant development. *Cell* 136: 1005–1016.
2. Kepinski S, Leyser O (2005) The *Arabidopsis* F-box protein TIR1 is an auxin receptor. *Nature* 435:446–451.
3. Dharmasiri N, Dharmasiri S, Estelle M (2005) The F-box protein TIR1 is an auxin receptor. *Nature* 435:441–445.
4. dos Santos Maraschin F, Memelink J, Offringa R (2009) Auxin-induced, SCF^{TIR1}-mediated poly-ubiquitination marks AUX/IAA proteins for degradation. *Plant J* 59: 100–109.
5. Tian Q, Reed JW (1999) Control of auxin-regulated root development by the *Arabidopsis thaliana SHY2/IAA3* gene. *Development* 126:711–721.
6. Hamann T, Benkova E, Bäurle I, Kientz M, Jürgens G (2002) The *Arabidopsis BODENLOS* gene encodes an auxin response protein inhibiting MONOPTEROS-mediated embryo patterning. *Genes Dev* 16:1610–1615.
7. Nelissen H, Boccardi TM, Himanen K, Van Lijsebettens M (2007) Impact of core histone modifications on transcriptional regulation and plant growth. *Crit Rev Plant Sci* 26: 243–263.
8. Nelissen H, et al. (2005) The *elongata* mutants identify a functional Elongator complex in plants with a role in cell proliferation during organ growth. *Proc Natl Acad Sci USA* 102:7754–7759.
9. Krogan NJ, Greenblatt JF (2001) Characterization of a six-subunit holo-Elongator complex required for the regulated expression of a group of genes in *Saccharomyces cerevisiae*. *Mol Cell Biol* 21:8203–8212.
10. Hawkes NA, et al. (2002) Purification and characterization of the human elongator complex. *J Biol Chem* 277:3047–3052.
11. Otero G, et al. (1999) Elongator, a multisubunit component of a novel RNA polymerase II holoenzyme for transcriptional elongation. *Mol Cell* 3:109–118.
12. Winkler GS, Kristjuhan A, Erdjument-Bromage H, Tempst P, Svejstrup JQ (2002) Elongator is a histone H3 and H4 acetyltransferase important for normal histone acetylation levels *in vivo*. *Proc Natl Acad Sci USA* 99:3517–3522.
13. Svejstrup JQ (2007) Elongator complex: How many roles does it play? *Curr Opin Cell Biol* 19:331–336.
14. Close P, et al. (2006) Transcription impairment and cell migration defects in Elongator-depleted cells: Implication for familial dysautonomia. *Mol Cell* 22:521–531.
15. Chen Y-T, et al. (2009) Loss of mouse *Ikbkap*, a subunit of Elongator, leads to transcriptional deficits and embryonic lethality that can be rescued by human *IKBKAP*. *Mol Cell Biol* 29:736–744.
16. Nelissen H, et al. (2003) DRL1, a homolog of the yeast TOT4/KTI12 protein, has a function in meristem activity and organ growth in plants. *Plant Cell* 15:639–654.
17. Gendrel A-V, Lippman Z, Martienssen R, Colot V (2005) Profiling histone modification patterns in plants using genomic tiling microarrays. *Nat Methods* 2:213–218.
18. Soppe WJJ, et al. (2002) DNA methylation controls histone H3 lysine 9 methylation and heterochromatin assembly in *Arabidopsis*. *EMBO J* 21:6549–6559.
19. Maere S, Heymans K, Kuiper M (2005) *BiNGO*: A cytoscape plugin to assess enrichment of Gene Ontology categories in biological networks. *Bioinformatics* 21:3448–3449.
20. Bennett T, et al. (2006) The *Arabidopsis MAX* pathway controls shoot branching by regulating auxin transport. *Curr Biol* 16:553–563.
21. Reinhardt D, et al. (2003) Regulation of phyllotaxis by polar auxin transport. *Nature* 426:255–260.
22. Donner TJ, Sherr I, Scarpella E (2009) Regulation of preprocambial cell state acquisition by auxin signaling in *Arabidopsis* leaves. *Development* 136:3235–3246.
23. Świątek A, Lenjou M, Van Bockstaele D, Inzé D, Van Onckelen H (2002) Differential effect of jasmonic acid and abscisic acid on cell cycle progression in tobacco BY-2 cells. *Plant Physiol* 128:201–211.
24. Lorenzo O, Solano R (2005) Molecular players regulating the jasmonate signalling network. *Curr Opin Plant Biol* 8:532–540.
25. Chen Z, et al. (2006) Mutation in ABO1/ELO2, a subunit of Holo-Elongator, increases abscisic acid sensitivity and drought tolerance in *Arabidopsis thaliana*. *Mol Cell Biol* 26:6902–6912.
26. Zhou X, Hua D, Chen Z, Zhou Z, Gong Z (2009) Elongator mediates ABA responses, oxidative stress resistance and anthocyanin biosynthesis in Arabidopsis. *Plant J* 60: 79–90.
27. Benhamed M, Bertrand C, Servet C, Zhou D-X (2006) *Arabidopsis GCN5, HD1*, and *TAF1/HAF2* interact to regulate histone acetylation required for light-responsive gene expression. *Plant Cell* 18:2893–2903.
28. Muse GW, et al. (2007) RNA polymerase is poised for activation across the genome. *Nat Genet* 39:1507–1511.
29. Fujita T, Puiz I, Schlegel W (2009) Negative elongation factor NELF controls transcription of immediate early genes in a stimulus-specific manner. *Exp Cell Res* 315: 274–284.
30. Benhamed M, et al. (2008) Genome-scale Arabidopsis promoter array identifies targets of the histone acetyltransferase GCN5. *Plant J* 56:493–504.
31. Bainbridge K, et al. (2008) Auxin influx carriers stabilize phyllotactic patterning. *Genes Dev* 22:810–823.
32. Cañas LA, Busscher M, Angenent GC, Beltrán J-P, van Tunen AJ (1994) Nuclear localization of the petunia MADS box protein FBP1. *Plant J* 6:597–604.
33. Fleury D, et al. (2007) The *Arabidopsis thaliana* homolog of yeast *BRE1* has a function in cell cycle regulation during early leaf and root growth. *Plant Cell* 19:417–432.
34. Van Leene J, et al. (2007) A tandem affinity purification-based technology platform to study the cell cycle interactome in *Arabidopsis thaliana*. *Mol Cell Proteomics* 6: 1226–1238.
35. Van Leene J, Witters E, Inzé D, De Jaeger G (2008) Boosting tandem affinity purification of plant protein complexes. *Trends Plant Sci* 13:517–520.
36. Bowler C, et al. (2004) Chromatin techniques for plant cells. *Plant J* 39:776–789.